ELSEVIER

Polymer 43 (2002) 369–387

polymer

www.elsevier.com/locate/polymer

Micromechanics of nanocomposites: comparison of tensile and compressive elastic moduli, and prediction of effects of incomplete exfoliation and imperfect alignment on modulus ☆

Douglas A. Brune, Jozef Bicerano*

The Dow Chemical Company, M.E. Pruitt Research Center, 1702 Building, Midland, MI 48674, USA

Abstract

This paper addresses three important aspects, neglected in all previous literature, of the micromechanics of nanocomposites reinforced by platelet-shaped fillers. (a) A model was developed to predict the buckling of platelets in reinforced materials under compressive loading. This model predicts a critical strain above which platelet buckling, and hence a reduction in the compressive modulus relative to the tensile modulus, would be expected to occur. It was used to show that compressive modulus should not be reduced relative to tensile modulus in a typical polypropylene nanocomposite. (b) A model was developed to account for the reduction of the reinforcement efficiency of clay platelets of high aspect ratio in a polymer matrix as a result of the incomplete exfoliation of platelets into 'pseudoparticle' stacks containing polymer layers sandwiched between successive clay platelet layers rather than into individual perfectly exfoliated and well-dispersed platelets. It was shown that incomplete exfoliation has a very significant detrimental effect on the reinforcement efficiency. (c) A model was also developed for the reduction of the reinforcement efficiency as a result of the deviation of the platelet orientation from perfect biaxial in-plane. It was shown that the deviation of the platelet orientation from perfect biaxial in-plane also has a very significant detrimental effect on the reinforcement efficiency.

Keywords: Nanocomposites; Micromechanics; Tensile and compressive elastic moduli

1. Introduction

Nanocomposites consisting of highly anisotropic clay platelets dispersed in a polymeric matrix material [1–16] are of interest for many important industrial applications. For example, polypropylene nanocomposites are currently under development for automotive fascia. The platelet-shaped clay nanofillers have thicknesses of ~1 nm. Their aspect ratios (defined as diameter/thickness) can range from 10 to 1000. Their elastic (Young's) moduli are $\sim 10^2$ times those of typical a thermoplastic or thermoset, and $\sim 10^5$ times those of a typical elastomer. The platelets occur naturally in stacks. These stacks must be torn apart (in other words, 'exfoliated'), to disperse them in the polymeric matrix as highly anisotropic nanofillers. The dispersion of such platelets improves many important properties, including the elastic moduli, relative to the polymeric matrix materials.

The development of nanocomposite technology presents many scientific challenges. A better fundamental understanding, and the ability to make predictions, are very important in accelerating the development of this technology. In particular, theory and simulations are especially useful in addressing the following three key research challenges:

- *Thermodynamics and kinetics of exfoliation*. This challenge is at the heart of the development of nanocomposite technology. Both the processing characteristics of the suspensions of clay platelets in polymers and the final properties of the fabricated articles made from these suspensions depend on the exfoliation and dispersion of the platelets. There is a significant amount of ongoing research in this area. For example, see Vaia and Giannelis [17,18] and Balazs et al. [19,20].
- *Rheology of dispersions of clay platelets in molten polymers*. The main objective of work in this area is to help optimize the processing characteristics during fabrication. The shear viscosity is of special interest. For example, see Bicerano et al. [21].
- *Elastic properties of nanocomposite fabricated articles.* Nanocomposite mechanics is not yet well-understood. This manuscript addresses, by developing analytical

☆ This paper was originally submitted to *Computational and Theoretical Polymer Science* and received on 27 March 2001; received in revised form on 20 July 2001; accepted on 20 July 2001. Following the incorporation of *Computational and Theoretical Polymer Science* into *Polymer*, this paper was consequently accepted for publication in *Polymer*.

* Corresponding author. Tel.: +1-517-636-6980; fax: +1-517-636-5406.
E-mail address: biceranoj@dow.com (J. Bicerano).

0032-3861/02/$ - see front matter
PII: S0032-3861(01)00543-2

(closed-form) solutions for the elasticity equations, what we consider to be the three most important aspects of the micromechanics of nanocomposites reinforced by platelet-shaped fillers that have been neglected in all of the previous literature.

Micromechanical methods use simplified geometries, thus neglecting complex geometrical features which could potentially be taken into account in numerical solutions of the elasticity equations by finite element simulations. They assume perfect adhesion (perfect load transfer) between the components in a composite, thus also neglecting interfacial phenomena, which could potentially be taken into account by mesoscale simulations. Nonetheless, they are extremely useful. Since the calculations are instantaneous, they provide the ability to assess rapidly the key factors controlling the elastic behavior, and to explore very large design spaces. Since the equations have closed-form solutions, the results can be related readily to geometrical and physical factors considered in the model.

The results reported in the remainder of this manuscript can be summarized as follows:

- A model was developed to predict the buckling of platelets in reinforced materials under compressive loading. This model predicts a critical strain above which platelet buckling, and hence a reduction in the compressive modulus relative to the tensile modulus, would be expected to occur. It was used to show that the compressive modulus should not be reduced relative to the tensile modulus in a typical polypropylene nanocomposite.
- A model was developed to account for the reduction of the reinforcement efficiency of clay platelets of high aspect ratio in a polymer matrix as a result of the incomplete exfoliation of platelets into 'pseudoparticle' stacks containing polymer layers sandwiched between successive clay platelet layers rather than into individual perfectly exfoliated and well-dispersed platelets. It was shown that incomplete exfoliation has a very significant detrimental effect on the reinforcement efficiency.
- A model was also developed for the reduction of the reinforcement efficiency as a result of the deviation of the platelet orientation from perfect biaxial in-plane. It was shown that the deviation of the platelet orientation from perfect biaxial in-plane also has a very significant detrimental effect on the reinforcement efficiency.

2. Prediction of threshold for decrease in compressive modulus relative to tensile modulus

2.1. Model development

Although dispersed clay platelets have a very high intrinsic stiffness (tensile moduli of $\sim 10^5$ MPa), their high aspect ratios induce large bending moments so that they manifest considerable flexibility [21]. Will a composite using fillers of high aspect ratio exhibit an enhanced compressive modulus in addition to an enhanced tensile modulus? To answer this question, we developed a model to predict the critical strain at which the compressive modulus of a composite reinforced by flexible filler particles begins to deviate from the tensile modulus. The model predicts the critical strain in terms of the moduli of the matrix and filler materials, and the volume fraction of filler. This section summarizes the model development and the results of illustrative calculations of the critical strain for dispersions of platelet-shaped filler particles in a typical grade of polypropylene (PP).

The overall strategy in developing the model was to write the elastic strain energy function for the composite material in terms of the physical properties of the matrix and the filler, the imposed strain, and the wavelength of any buckling of the composite material. The behavior of the strain energy function was then examined to see under what circumstances the low-energy conformation was the linear compression of both the matrix and the filler (which produces a compressive modulus equal to the tensile modulus), and under what circumstances buckling would occur (reducing the compressive modulus). This strategy is similar to an approach used to predict the failure of sandwich panels under compressive loading [22], a common reference in materials books which touch on the subject of compressive loading of composites [23].

In the derivation below and the illustrative application that follows it, the bulk material properties of the matrix polymer were used to represent this material. This is, strictly speaking, an approximation because of the effects of the large interfacial area and the nanoscale dimensions in nanocomposites. Such issues will be addressed in considerable detail in Section 5. It suffices to state, at this point, that we believe that taking these factors into account (which would require a large amount of additional work) is very unlikely to change the qualitative conclusions that are reached in this section concerning the threshold for the decrease in the compressive modulus relative to the tensile modulus.

In examining the behavior of materials reinforced with platelet-shaped filler particles, we made some assumptions to make the calculations easier and to provide a reasonable lower bound for the critical strain at which the compressive modulus begins to deviate from the tensile modulus. Since our lower bound showed a very high critical strain for the case of greatest interest to us, there was no need to refine these assumptions. These assumptions are that (1) the composite stores energy via compression of filler and matrix, as well as shear of the matrix if the filler buckles; (2) filler particles are initially aligned with the applied load; and (3) that initial filler buckling would result in composite deformation that follows a sinusoidal pattern. With these assumptions, the detailed derivation of the critical strain,

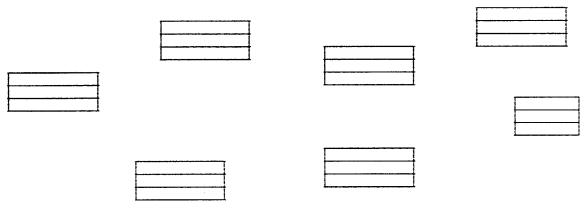

Fig. 1. If exfoliation is incomplete, we can consider the system as a composite which consists of a matrix and 'pseudoparticles' which are incompletely exfoliated stacks of individual platelets. The Halpin–Tsai equations can then be applied to this model system, which is depicted schematically in this figure. The solid lines represent platelets within incompletely exfoliated stacks. The dashed rectangles illustrate where the boundaries of a pseudoparticle are drawn to apply the Halpin–Tsai Equations in a generalized form.

contained in Appendix A, results in the relation:

$$e_{crit} = \frac{G_{matrix}(1-\phi)}{E_{filler}\phi} = \left(\frac{E_{matrix}}{E_{filler}}\right)\left(\frac{1}{2(1+\nu_{matrix})}\right)\left(\frac{1-\phi}{\phi}\right)$$

where G_{matrix} is the matrix shear modulus, E_{filler} is the filler Young's Modulus, and ϕ is the volume fraction filler.

2.2. Example

The critical strain for the onset of filler buckling in a PP nanocomposite containing 5% filler by volume will now be computed. For this system,

$$\frac{E_{matrix}}{E_{filler}} = \frac{1360\ \text{MPa}}{100\,000\ \text{MPa}} = 0.0136$$

$$\frac{1}{2(1+\nu_{matrix})} = \frac{1}{2(1+0.4)} = 0.357$$

$$\frac{1-\phi}{\phi} = \frac{1-0.05}{0.05} = 19$$

$$e_{crit} = (0.0136)(0.357)(19) = 0.09$$

This strain is quite large. The matrix stress corresponding to this strain, 95.2 MPa, is far greater than the elastic limit of the PP matrix, 25 MPa. This result shows that the PP matrix will undergo plastic deformation before the filler starts to buckle, so that the elastic compressive modulus will not be reduced relative to the elastic tensile modulus.

On the other hand, filler buckling would be far more likely to occur in a soft elastomeric matrix where the ratio E_{matrix}/E_{filler} is roughly three orders of magnitude smaller than that calculated above for the stiff thermoplastic PP matrix.

3. Prediction of effects of incomplete exfoliation on tensile modulus

3.1. Model development

It is obvious from electron micrographs that one often has incompletely exfoliated stacks of platelets, containing some organocation and/or matrix polymer between the platelets in each stack. Such stacks can contain several platelets, and the platelets within a stack can be at various distances from each other. An important issue, which may have drastic effects on the reinforcement efficiency, is the point in the interlayer expansion of a stack with a given number of layers at which a stack becomes a collection of separate exfoliated platelets of high A_f and Young's modulus of E at a volume fraction of ϕ, rather than behaving like a single 'pseudoparticle'. A pseudoparticle would have a lower 'effective' aspect ratio A_f' (because of stacking), and a lower Young's modulus E' as well as a higher volume fraction ϕ' (because of its trapped organic fraction). A standard technique of composite theory that is used routinely to estimate reinforcement effects, the Halpin–Tsai equations [25], will be modified below to account for these effects.

In a completely exfoliated system, the 'continuum' Halpin–Tsai Equations can be applied to predict the modulus of the composite material:

$$\frac{E_{composite}}{E_{matrix}} = \frac{1+2A_f\eta\phi}{1-\eta\phi},$$

where A_f is the aspect ratio of the platelet (>1 if we define A_f as diameter divided by thickness for cylindrical platelets), ϕ is the volume fraction of platelets in the composite, and η is given by:

$$\eta = \frac{E_r - 1}{E_r + 2A_f},$$

where E_r is the ratio of the platelet to the matrix modulus.

If exfoliation is incomplete, we can consider the system as a composite which consists of a matrix and pseudoparticles which are incompletely exfoliated stacks of individual platelets. The Halpin–Tsai equations can then be applied to this model system, which is depicted schematically in Fig. 1. Here, the solid lines represent the platelets within incompletely exfoliated stacks, and the dashed rectangles illustrate where the boundaries of a pseudoparticle are drawn to apply the Halpin–Tsai Equations in the following generalized form:

$$\frac{E_{composite}}{E_{matrix}} = \frac{1+2A_f'\eta'\phi'}{1-\eta'\phi'}, \qquad \eta' = \frac{E_r' - 1}{E_r' + 2A_f'},$$

where A_f' is now the aspect ratio of the platelet stack, ϕ' the volume fraction of platelet stacks in matrix, and E_r' is the ratio of the modulus of the platelet stack to that of the matrix. In Appendix B, each of these primed quantities is evaluated from

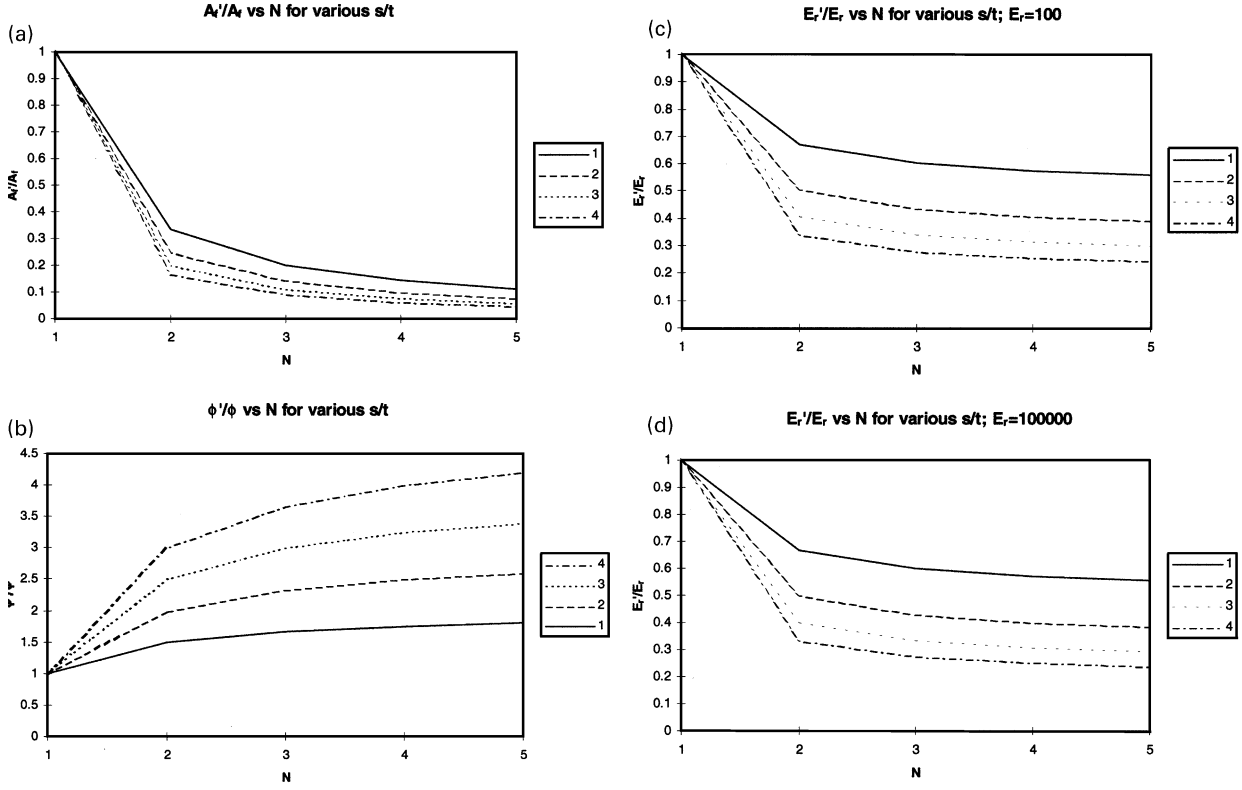

Fig. 2. Effects of N (number of platelets per stack) and s/t (ratio of platelet spacing to platelet thickness in a stack) on (a) the aspect ratio, (b) volume fraction, and (c) modulus ratio in the Halpin–Tsai equations, as ratios of the modified divided by unmodified terms.

the geometry of the stacks. The resulting set of equations are:

$$\frac{E_{\text{composite}}}{E_{\text{matrix}}} = \frac{1 + 2A_{\text{f}}'\eta'\phi'}{1 - \eta'\phi'}, \qquad \eta' = \frac{E_{\text{r}}' - 1}{E_{\text{r}}' + 2A_{\text{f}}'},$$

$$A_{\text{f}}' = \frac{A_{\text{f}}}{\hat{N}}\left(\frac{1}{1 + (1 - 1/\hat{N})\dfrac{s}{t}}\right)$$

$$\phi' = \phi\left(1 + (1 - 1/\hat{N})\frac{s}{t}\right)$$

$$E_{\text{r}}' = E_{\text{r}}\left(\frac{1}{1 + (1 - 1/\hat{N})\dfrac{s}{t}}\right) + \frac{(1 - 1/\hat{N})\dfrac{s}{t}}{1 + (1 - 1/\hat{N})\dfrac{s}{t}}$$

$$\hat{N} = N + (1 - N)\left(\frac{s}{t}\right)\left(\frac{\phi}{1 - \phi}\right).$$

3.2. Examples

Fig. 2 shows the effects of N (number of platelets per stack) and s/t (ratio of platelet spacing to platelet thickness in a stack) on the aspect ratio, volume fraction, and modulus ratio in the Halpin–Tsai equations as ratios of the modified divided by unmodified terms:

- Fig. 2(a) is the ratio of the aspect ratio of the stacks to that of individual platelets ($A_{\text{f}}'/A_{\text{f}}$). Both N and s/t play important roles. As more platelets are incorporated into a stack, or as platelet spacing increases, the aspect ratio of the stack falls.
- Fig. 2(b) is the ratio of the volume fraction of platelet stacks to that of individual platelets (ϕ'/ϕ). Again, both N and s/t play important roles. As more platelets are incorporated into a stack, or as platelet spacing increases, more matrix material is incorporated into the stacks, and the volume fraction of the stacks increases.
- Fig. 2(c) and (d) show the ratio of the stack modulus to the platelet modulus ($E_{\text{r}}'/E_{\text{r}}$, with matrix modulus cancelling). Although the structure of the equations suggests that the results might vary as the platelet modulus ratio (E_{r}) is changed, the plots at $E_{\text{r}} = 100$ [typical order of magnitude for inorganic platelets dispersed in a rigid (thermoplastic or thermoset) matrix] and $E_{\text{r}} = 100\,000$ [typical order of magnitude for inorganic platelets dispersed in a soft (elastomeric) matrix] show almost no difference. This is due to the fact that at these values of E_{r}, the part of the $E_{\text{r}}'/E_{\text{r}}$ ratio which depends on E_{r} is insignificant compared to the part which does not. These results also imply that, so long as there is enough adhesion to transfer a load, the presence of an even softer material (such as an organocation) instead of a polymer in the interlayer space of the stacks should not make a qualitatively significant difference in the results. It is

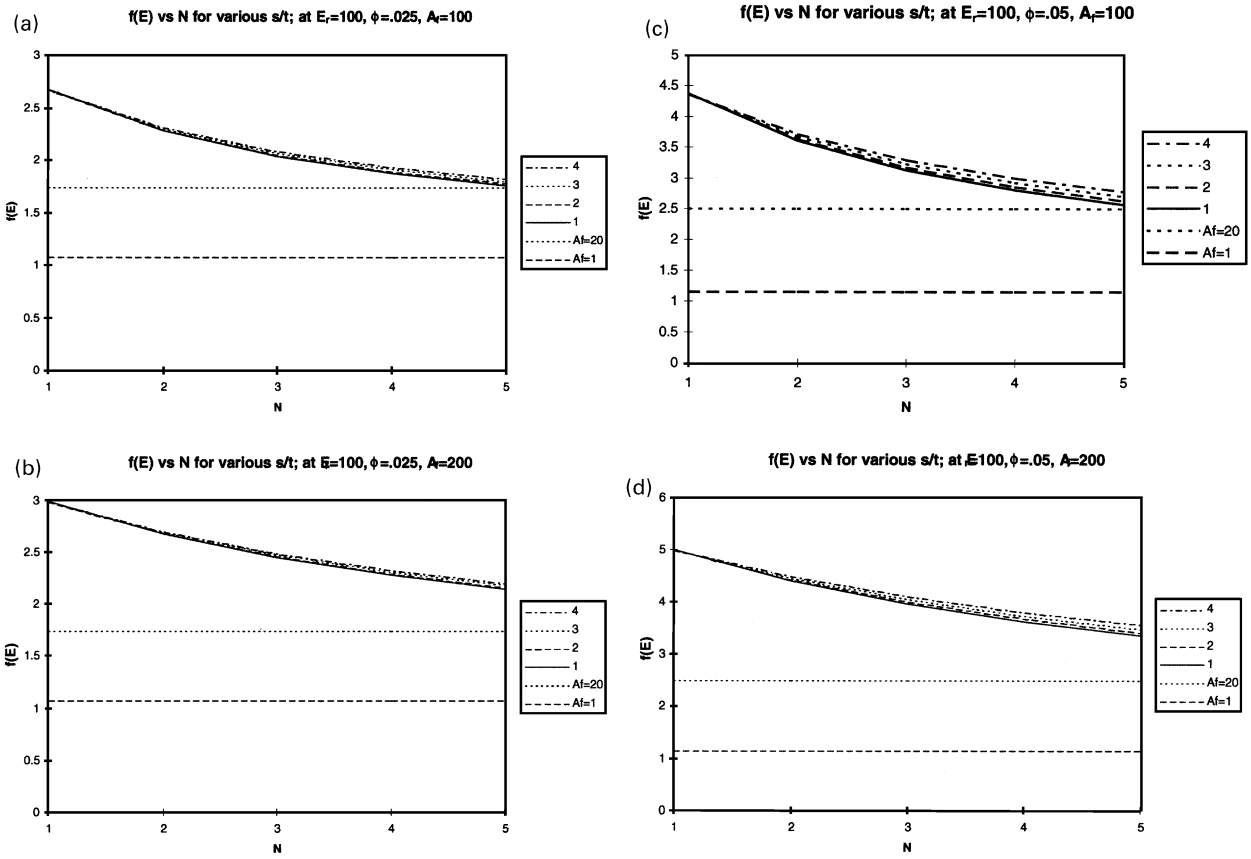

Fig. 3. Ratio of composite modulus to matrix modulus, *f(E)*, as a function of number *N* of platelets in a typical stack, for *s*/*t* ratios of 1, 2, 3, and 4. The *s*/*t* ratio represents the ratio of the distance between the platelets in a stack to the platelet thickness. For well-exfoliated platelets ($N = 1$), *f(E)* equals the results obtained by using the continuum Halpin–Tsai equations. The eight graphs represent all possible combinations of the following parameters: (a) platelet volume fraction, ϕ, equal to 0.025 and 0.05; (b) platelet aspect ratio, A_f, equal to 100 and 200; and (c) ratio of platelet to matrix modulus, E_r, equal to 100 and 100000. Dashed reference lines corresponding to *f(E)* values calculated for platelets of aspect ratio 1 (cylinders with height = diameter) and 20 (as in conventional unexfoliated platelet-shaped fillers such as talc or mica flakes) are also shown.

seen that increasing the number of platelets per stack does very little to change E_r'/E_r after a large change from individual platelets to two-platelet stacks. Increasing *s*/*t* makes a larger difference, reflecting the incorporation of larger amounts of the softer matrix material into platelet stacks.

Fig. 3 shows the ratio of the composite modulus to the matrix modulus, $f(E)$, as a function of the number N of platelets in a typical stack, for *s*/*t* ratios of 1, 2, 3, and 4. The *s*/*t* ratio represents the ratio of the distance between the platelets in a stack to the platelet thickness. For well-exfoliated platelets ($N = 1$), $f(E)$ equals the results obtained by using the continuum Halpin–Tsai equations. The eight graphs of Fig. 3 represent all possible combinations of the following parameters: (a) platelet volume fraction, ϕ, equal to 0.025 and 0.05; (b) platelet aspect ratio, A_f, equal to 100 and 200; and (c) ratio of platelet to matrix modulus, E_r, equal to 100 and 100 000. Dashed reference lines corresponding to the $f(E)$ values calculated for platelets of aspect ratio 1 (cylinders with height = diameter) and 20 (as in conventional unexfoliated platelet-shaped fillers such as talc or mica flakes) are also shown. A striking aspect of the results shown in Fig. 3, the weak dependence on *s*/*t*, is somewhat surprising since it was shown in Fig. 2 that all the terms of the Halpin–Tsai equations are affected significantly by *s*/*t*.

4. Prediction of effects of off-plane deviations of platelet orientation on tensile modulus

4.1. Earlier version of model used for micromechanical calculations

Within Dow, the program used to compute elastic moduli of a reinforced (filled) material is called LITAC[1]. It uses information about filler and matrix moduli, filler geometry, and orientation to compute composite properties with the

[1] The original version of LITAC was developed by Professor Charles L. Tucker from the University of Illinois in Urbana-Champaign and Dr Randy S. Bay (at the time a graduate student of Professor Tucker) in a cooperative research project funded by Dow to acquire the capability to predict the thermoelastic properties of composites. The software was accompanied by a Theory Manual and a User's Manual providing extensive documentation about the methods and the software.

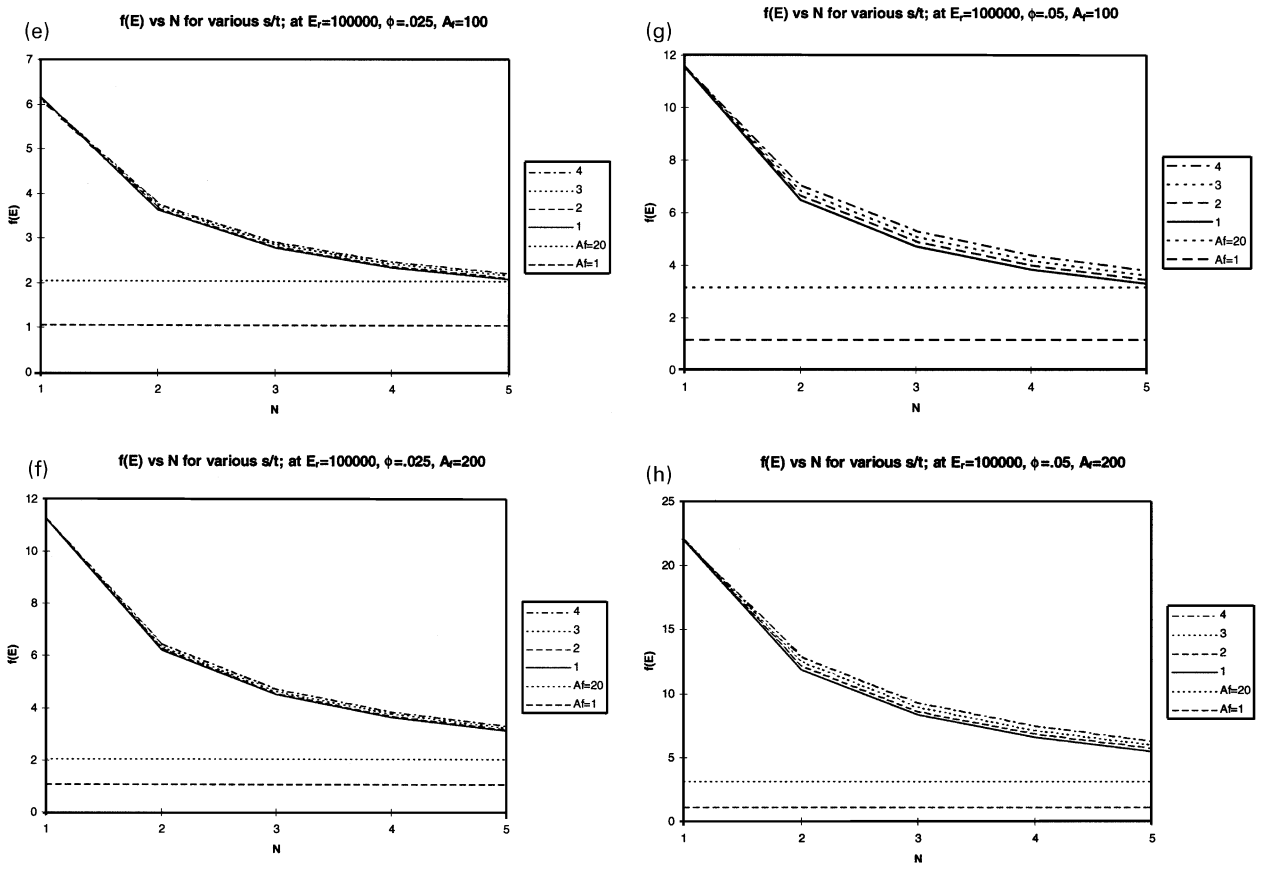

Fig. 3. (*continued*)

Halpin–Tsai equations [25,26]. It can be used to calculate composite properties in any chosen direction, for filler orientations described by any given distribution function. In order to do these calculations, however, LITAC relies on property calculations for perfectly aligned rod-shaped or disk-shaped particles. To fully describe the material response (and thus to be able to calculate the composite properties in any given direction), five independent elastic constants are required. The five elastic constants calculated by LITAC are the Young's modulus for applied stress parallel and orthogonal to the particle symmetry axis, the shear modulus for stresses in planes containing and orthogonal to the particle symmetry axis, and the Poisson's ratio for stress parallel to the particle symmetry axis.

LITAC calculations for rod-shaped particles follow fairly well-established formulas. However, for disk-shaped particles, LITAC has two independent estimation methods, one for very low aspect ratio particles, and another, which can be applied to a broad range of aspect ratios. The two methods can lead to very different results for the Young's modulus for stress parallel to the particle symmetry axis. We will now develop a way to unify the LITAC computations for a material reinforced with disk-shaped particles. We then apply the new method to determining the moduli of typical nanocompsite reinforced materials, as a function of the orientation of the nanocomposite filler particles. In this section, the aspect ratio of a cylindrical particle will be defined as (height/diameter), so that it will be >1 for rod-shaped fillers but <1 for disk-shaped fillers.

A material reinforced by perfectly aligned rod or disk shaped particles exhibits composite elastic properties which vary, depending on the orientation of the applied stress. Because of the alignment of the particles and their symmetry, however, the compliance tensor contains only five independent components. The compliance matrix, S (a standard way to relate strain to stress; see Ref. [25] and footnote 1 for a complete description of the notation, and the relationships between stiffness and compliance matrices and tensors), can be expressed in terms of five independent elastic constants, E_1, E_2, G_{12}, G_{23} and ν_{12}, as follows:

$$\epsilon S\sigma, \qquad \sigma = \begin{bmatrix} \sigma_{11} \\ \sigma_{22} \\ \sigma_{33} \\ \sigma_{23} \\ \sigma_{31} \\ \sigma_{12} \end{bmatrix}, \qquad \epsilon = \begin{bmatrix} \epsilon_{11} \\ \epsilon_{22} \\ \epsilon_{33} \\ 2\epsilon_{23} \\ 2\epsilon_{31} \\ 2\epsilon_{12} \end{bmatrix}$$

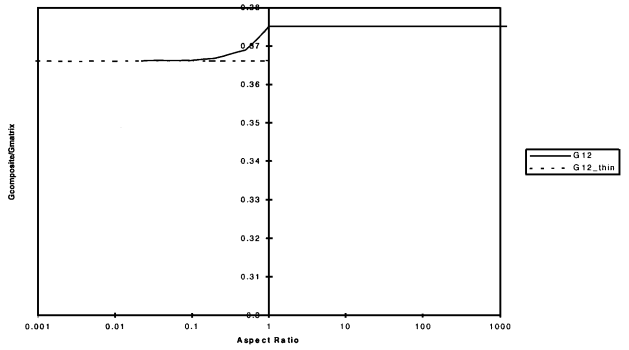

Fig. 4. For shear modulus in the 1–2 or 1–3 plane, LITAC uses the Halpin–Tsai formula. As aspect ratio approaches zero, its results approach the infinitely thin disk solution for G_{12}. A representative plot is shown; for $\phi = 0.025$, $E_r = 100$, and $\nu_m = \nu_f = 0.4$.

$$S = \begin{bmatrix} \frac{1}{E_1} & \frac{-\nu_{12}}{E_1} & \frac{-\nu_{12}}{E_1} & 0 & 0 & 0 \\ \frac{-\nu_{12}}{E_1} & \frac{1}{E_2} & \frac{-\nu_{23}}{E_2} & 0 & 0 & 0 \\ \frac{-\nu_{12}}{E_1} & \frac{-\nu_{23}}{E_2} & \frac{1}{E_2} & 0 & 0 & 0 \\ 0 & 0 & 0 & \frac{1}{G_{23}} & 0 & 0 \\ 0 & 0 & 0 & 0 & \frac{1}{G_{12}} & 0 \\ 0 & 0 & 0 & 0 & 0 & \frac{1}{G_{12}} \end{bmatrix},$$

$$G_{23} = \frac{E_2}{2(1 + \nu_{23})}.$$

An examination of the compliance matrix shows that the '1' direction is special: this is the direction in which the symmetry axis of the particle points. Rather than three independent shear moduli, there are only two: one for shear stress in the plane containing the particle symmetry axis (G_{12}), one for shear stress in the plane orthogonal to it (G_{23}). The Young's modulus shows similar symmetry: there are two independent values, one for normal stress along the particle symmetry axis (E_1), and another for normal stress orthogonal to the particle symmetry axis (E_2).

4.2. Rod-shaped particles (fibers)

For rod-shaped particles, LITAC follows the Halpin–Tsai equations to calculate the five elastic constants. The Young's moduli are calculated using:

$$E_x = \frac{1 + \xi\eta\phi}{1 - \eta\phi}, \qquad \eta = \frac{E_r - 1}{E_r + \xi}$$

with $\xi = 2A_f = 2$ length/diameter for Young's modulus along the particle symmetry axis (E_1), and $\xi = 2$ for Young's modulus orthogonal to the symmetry axis (E_2). In these equations, E_r is the ratio of the Young's modulus for the filler to Young's modulus for the matrix, and ϕ is the volume fraction filler.

The shear moduli are:

$$G_{xy} = \frac{1 + \xi\eta\phi}{1 - \eta\phi}, \qquad \eta = \frac{G_r - 1}{G_r + \xi},$$

where G_r is the ratio of the shear modulus for the filler to the shear modulus for the matrix; and $\xi = 1$ for shear in the 1–3 or 1–2 planes, and

$$\xi = \frac{\frac{K_m}{G_m}}{\frac{K_m}{G_m} + 2}, \qquad K_m = \frac{E_m}{3(1 - 2\nu_m)},$$

for shear in the 2–3 plane.

Finally, LITAC uses a simple mixing rule to estimate ν_{12}:

$$\nu_{12} = \phi\nu_f + (1 - \phi)\nu_m.$$

This mixing rule is used by Halpin and Tsai as an approximation during the derivation of their formulas for E_1, E_2, G_{12}, and G_{23}.

It is interesting to examine these calculations in the limit of spherical particles. In this limit the composite is isotropic and the following must be true: $E_1 = E_2 = E$, $G_{12} = G_{23} = G$, $\nu_{12} = \nu$, and $G = E/2/(1 + \nu)$. The first relation, $E_1 = E_2 = E$, is satisfied by the LITAC formulas. The last three relations give three possible ways of calculating G for the composite: using the formula for G_{12}, the formula for G_{23}, or the formulas for E and ν_{12}. Carrying out several example calculations shows that although the G calculated by the three methods is different, the difference is small. For example, for $\phi = 0.025$, $E_r = 100$, and $\nu_m = \nu_f = 0.4$; $G_r = G_{12}/G_m = 1.05$, $G_r = G_{23}/G_m = 1.04$, and $G_r = E/2/(1 + \nu)/G_m = 1.07$.

4.3. Disk-shaped particles (platelets)

For disk-shaped particles, LITAC includes two options: one for infinitely thin disks, and one for disks of finite aspect ratio. The option for infinitely thin disks uses the results from a micromechanics-based solution. The option for disks of finite aspect ratio pieces together a number of different results. Each elastic constant will now be examined.

For shear modulus in the 1–2 or 1–3 plane, LITAC uses the Halpin–Tsai formula:

$$G_{12} = \frac{1 + \xi\eta\phi}{1 - \eta\phi}, \qquad \eta = \frac{G_r - 1}{G_r + \xi},$$

$$\xi = 2\left(\frac{\text{thickness}}{\text{diameter}}\right)^{1.732}.$$

As aspect ratio approaches zero, this formula gives results which approach the infinitely thin disk solution for G_{12}. A

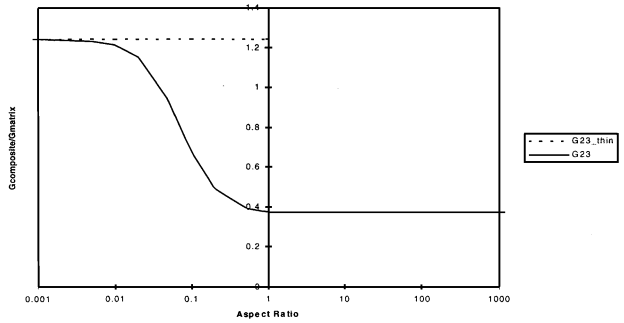

Fig. 5. For shear modulus in the 2–3 plane, LITAC reverses the thickness/diameter ratio in the equation for G_{12}. This gives the usual Halpin–Tsai result for spherical particles (where the composite is isotropic, so $G_{23} = G_{12}$), and also approaches the infinitely thin disk solution as aspect ratio approaches zero. A representative plot is shown, using the same parameters as in Fig. 4.

representative plot is shown in Fig. 4, for $\phi = 0.025$, $E_r = 100$, and $\nu_m = \nu_f = 0.4$.

Fig. 4 shows that there is some irregular behavior near aspect ratio 1 (spheres), but considering the slow variation in G_{12} (0.366–0.375 over the entire range of aspect ratios), it was not considered necessary to correct this.

For shear modulus in the 2–3 plane, LITAC does not use the usual recommended Halpin–Tsai formula [26], but simply reverses the thickness/diameter ratio in the equation for G_{12}. This gives the usual Halpin–Tsai result for spherical particles (where the composite is isotropic, so $G_{23} = G_{12}$), and also approaches the infinitely thin disk solution as aspect ratio approaches zero. A representative plot is shown in Fig. 5, using the same parameters as in Fig. 4. There is a slight discontinuity at aspect ratio 1 (spheres) caused by the fact that the LITAC formulas for disks give $G_{23} = G_{12}$ in the sphere limit, while the LITAC formulas for rods (as discussed above) do not.

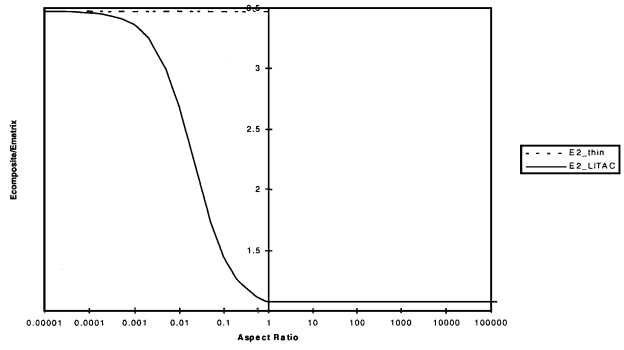

Fig. 6. For Young's modulus orthogonal to the particle symmetry axis (E_2), LITAC uses the recommended Halpin–Tsai equation. For aspect ratios which approach zero, this formula gives results which are exactly equal to the infinitely thin disk solution, provided that Poisson's ratio for the matrix is equal to that for the filler. If the Poisson's ratios are not equal, the limit is close to but not exactly equal to the thin disk solution. The results of this calculation are shown, using the same parameters as in Fig. 4 except that Poisson's ratio for the filler was decreased from 0.4 to 0.3 to illustrate the small magnitude of the discrepancy between the Halpin–Tsai and thin-disk solutions.

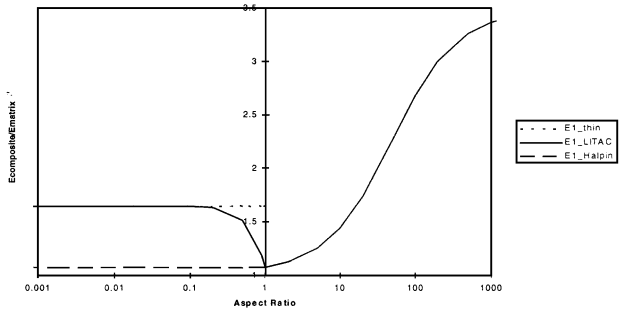

Fig. 7. E_2/E_{matrix} over the full disk–sphere–rod range of aspect ratios, as calculated by the Halpin–Tsai equations, and as modified by LITAC to honor the infinitely thin disk solution. Parameters for this plot are the same as those for Fig. 4.

For Young's modulus orthogonal to the particle symmetry axis (E_2), LITAC uses the recommended Halpin–Tsai equation:

$$E_2 = \frac{1 + \xi\eta\phi}{1 - \eta\phi}, \qquad \eta = \frac{E_r - 1}{E_r + \xi},$$

$$\xi = \frac{2}{A_f} = 2\frac{\text{diameter}}{\text{thickness}}.$$

For aspect ratios which approach zero, this formula gives results which are exactly equal to, the infinitely thin disk solution, provided that Poisson's ratio for the matrix is equal to that for the filler. If the Poisson's ratios are not equal, the limit is close to but not exactly equal to the thin disk solution. The results of this calculation are shown in Fig. 6, using the same parameters as in Fig. 4 except that Poisson's ratio for the filler was decreased from 0.4 to 0.3 to illustrate the small magnitude of the discrepancy between the Halpin–Tsai and thin-disk solutions.

For Young's modulus along the particle symmetry axis (E_1), Halpin [26] recommends that the equation for E_2 be used, with ξ set to 2. This results in a Young's modulus equal to that for spheres, regardless of the aspect ratio of the reinforcing particles. LITAC does not implement this recommendation, because it leads to large disagreements with the infinitely thin disk solution. In an effort to honor both the Halpin–Tsai equation for spheres, and the analytical solution for infinitely thin disks, LITAC uses the square of the particle aspect ratio to interpolate between these two limits.

Fig. 7 shows E_2/E_{matrix} over the full disk–sphere–rod range of aspect ratios, as calculated by the Halpin–Tsai equations, and as modified by LITAC to honor the infinitely thin disk solution. Parameters for this plot are the same as those for Fig. 4. A weakness in the LITAC calculation for E_1 is seen: the method of interpolation between the sphere limit and the infinitely thin disk limit leads to non-smooth results in the region near spheres. While we don't expect exact symmetry, we should expect smoother behavior than this. Why is this important? The method of interpolation can lead

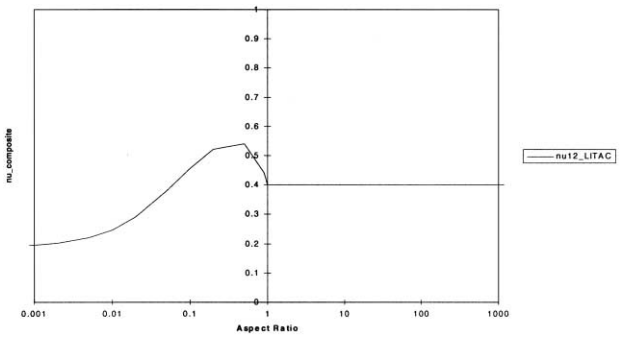

Fig. 8. To calculate ν_{12}, LITAC assumes that ν_{21} can be approximated by the rule of mixtures over the whole range of aspect ratios, then uses the identity $E_2\nu_{12} = E_1\nu_{21}$ together with calculated values for E_1 and E_2. The results of this calculation are shown, using the same parameters as in Fig. 4.

to substantial differences in the modulus for the aspect ratios in which we are interested.

To calculate ν_{12}, LITAC assumes that ν_{21} can be approximated by the rule of mixtures over the whole range of aspect ratios (based on the fact that it is a pretty good approximation for both spheres and infinitely thin disks), then uses the identity $E_2\nu_{12} = E_1\nu_{21}$ together with calculated values for E_1 and E_2. The results of this calculation are shown in Fig. 8, using the same parameters as in Fig. 4. Fig. 8 shows that the LITAC calculation for ν_{12} suffers from the interpolation procedure which caused irregular behavior in E_1.

In the limit of spherical particles, $E_1 = E_2$, so $\nu_{12} = \nu_{21}$, and both are given by the assumed rule of mixtures, which agrees with the LITAC result for rods. As before with rods, it is possible to check the isotropic identity $G = E/2/(1 + \nu)$ is satisfied in the sphere limit. Again the results for calculating G from the LITAC formulas for ν_{12} and E are close, but not quite equal, to those calculated from the formulae for G_{12} and G_{23}.

4.4. Refinements needed for disk-shaped particles in earlier version of model

Reviewing the figures showing the LITAC calculation results, the following is clear:

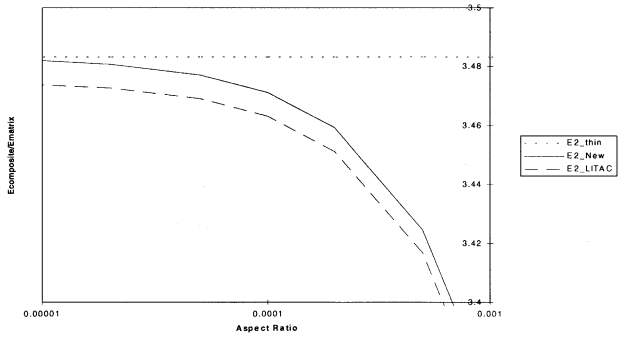

Fig. 9. The refined equation for E_2 is plotted for low aspect ratios, showing that it correctly reaches the infinitely thin disk solution.

- The LITAC results for the shear moduli provide reasonable ways of interpolating between the known limits for spheres and infinitely thin disks (which are not that far apart to begin with).
- The LITAC calculation for E_2 needs some minor repair to make it agree with the thin disk solution.
- The LITAC calculation for E_1 needs major surgery to provide a better method of interpolation between the known limits.
- The LITAC calculation for ν_{12} needs a reasonable input for E_1, in order to provide reasonable results.

4.5. Refinements in E_2 calculation for disk-shaped particles

Because the high aspect ratio limit of the Halpin–Tsai equation for E_2 is so close to the micromechanics solution for infinitely thin disks, it is safe to assume that the Halpin–Tsai equation captures the aspect ratio dependence. All that is necessary is to adjust the limiting behavior slightly, so that the solutions will match. To accomplish this, consider the following identity:

$$\frac{E_2(A_f) - E_2(1)}{E_2(1/\infty) - E_2(1)} = \frac{E_2(A_f) - E_2(1)}{E_2(1/\infty) - E_2(1)}$$

which can be rearranged to

$$E_2(A_f) = E_2(1) + [E_2(1/\infty) - E_2(1)]\left[\frac{E_2(A_f) - E_2(1)}{E_2(1/\infty) - E_2(1)}\right]$$

$$= E_2(1) + [E_2(1/\infty) - E_2(1)] \times INTERP2$$

The quantity on the left-hand side of the equation is the thing were trying to calculate, E_2 as a function of aspect ratio, A_f. On the right-hand side, the quantities $E_2(1/\infty)$ and $E_2(1)$ are the known solutions for infinitely thin disks and spheres, respectively. The last quantity in square brackets can be viewed as an interpolating function, call it *INTERP*2; in our case, if we use the Halpin–Tsai calculation for E_2 to compute all the terms in this function, we will produce an equation that behaves like the Halpin–Tsai equation, but approaches the infinitely thin disk result instead of the Halpin–Tsai limit, as aspect ratio approaches $1/\infty$. When the Halpin–Tsai results are substituted into the formula for *INTERP*2, the result is:

$$INTERP2 = \left[\frac{\xi - 2}{(E_r - 1)(1 - \phi) + (1 + \xi)}\right],$$

$$E_r = \frac{E_{filler}}{E_{matrix}}, \qquad \xi = \frac{2}{A_f} = 2\frac{\text{diameter}}{\text{thickness}}.$$

So the equation for estimating E_2 for disk shaped filler particles becomes:

$$E_2(A_f) = E_2(1) + [E_2(1/\infty) - E_2(1)]$$

$$\times\left[\frac{\xi - 2}{(E_r - 1)(1 - \phi) + (1 + \xi)}\right],$$

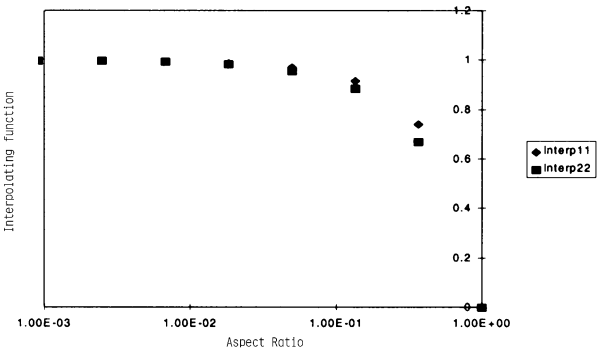

Fig. 10. The behavior of the interpolation functions *INTERP*1 and *INTERP*2.

where, as before $E_2(1/\infty)$ is the solution for infinitely thin disks, and $E_2(1)$ is the solution for spheres. This equation for E_2 is plotted for low aspect ratios in Fig. 9, showing that it correctly reaches the infinitely thin disk solution.

4.6. Refinements in E_1 calculation for disk-shaped particles

In calculating E_1, the LITAC concept of interpolating between well-known solutions is a good one; we just need to find a better method of interpolation. To see what we are after, consider the following identity:

$$\frac{E_1(A_f) - E_1(1)}{E_1(1/\infty) - E_1(1)} = \frac{E_1(A_f) - E_1(1)}{E_1(1/\infty) - E_1(1)}$$

which can be rearranged to

$$E_1(A_f) = E_1(1) + [E_1(1/\infty) - E_1(1)]\left[\frac{E_1(A_f) - E_1(1)}{E_1(1/\infty) - E_1(1)}\right]$$

$$= E_1(1) + [E_1(1/\infty) - E_1(1)] \times INTERP1$$

The quantity on the left-hand side of the equation is our unknown. On the right-hand side, the quantities $E_1(1/\infty)$ and $E_1(1)$ are the known solutions for infinitely thin disks and spheres, respectively. The last quantity in square brackets can be viewed as an interpolating function, call it *INTERP*1: we need to find a function that behaves similarly as aspect ratio decreases from *1* to $1/\infty$.

How can we do this? If we knew the behavior of *INTERP*1, then we wouldn't need to find something to approximate it, because we'd already have the answer to our problem! We used one approach in adjusting the limiting behavior of E_2 above: we used the Halpin–Tsai equations for E_2 to interpolate between the known solutions for spheres and infinitely thin disks. For E_1, it is not possible to do this, because the Halpin–Tsai equations predict *no* aspect ratio dependence for E_1. Another approach is to find a class of problems for which we *do* know the behavior of *INTERP*1, then find a good approximation for *INTERP*1 which can be calculated under all conditions.

Where can we find a class of problems that allows solution for *INTERP*1? In the limit of low volume fraction, for rigid ellipsoidal fillers of all aspect ratios, [27] shows how to compute the matrix deformation at all points in space for a linear applied strain field. We can use this solution to compute effective moduli for the composite materials. The details of this computation are extremely complex and are shown in Appendix C. Two highlights from these results follow:

1. The solution is known to be valid only in the regime of very low volume fraction. How low is low? It depends on the aspect ratio of the filler particles. As particle aspect ratio increases, the cutoff volume fraction decreases. To ensure that we are examining only the aspect ratio contribution, it is necessary to examine the behavior of the following quantity, rather than E_1 itself:

$$[E_1] = \lim_{\phi \to 0}\left(\frac{E_1 - E_{matrix}}{\phi}\right).$$

2. Since the solution is for completely rigid fillers, $[E_1]$ does not approach a finite value as aspect ratio gets very large. The limiting behavior is an asymptotic approach to $1/A_f$. In order to have a meaningful computation of *INTERP*1, it is necessary to scale out the asymptotic behavior by dividing by the asymptote. The resulting quantity then measures the rate of approach to the high aspect ratio asymptote, which is what we want.

This is half of the story. The other half is finding a useful approximation for *INTERP*1. Without going into the details of the search, here is the result:

$$INTERP1 = \left[\frac{E_1(A_f) - E_1(1)}{E_1(1/\infty) - E_1(1)}\right] \cong \left[\frac{E_2(A_f) - E_2(1)}{E_2(1/\infty) - E_2(1)}\right]$$

$$= INTERP2$$

The behavior of *INTERP*1 and *INTERP*2 is shown in Fig. 10. It can be seen that *INTERP*1 and *INTERP*2 differ by less than 10% over the range of interest, which makes *INTERP*2 a good candidate to replace *INTERP*1. *INTERP*2 can also be calculated in the more general case, from the appropriate Halpin–Tsai equations. When the Halpin–Tsai results are substituted into the formula for *INTERP*2, the result is:

$$INTERP2 = \left[\frac{\xi - 2}{(E_r - 1)(1 - \phi) + (1 + \xi)}\right],$$

$$E_r = \frac{E_{filler}}{E_{matrix}}, \qquad \xi = \frac{2}{A_f} = 2\frac{\text{diameter}}{\text{thickness}}.$$

So the equation for estimating E_1 for disk-shaped filler particles becomes:

$$E_1(A_f) = E_1(1) + [E_1(1/\infty) - E_1(1)]$$

$$\times\left[\frac{\xi - 2}{(E_r - 1)(1 - \phi) + (1 + \xi)}\right],$$

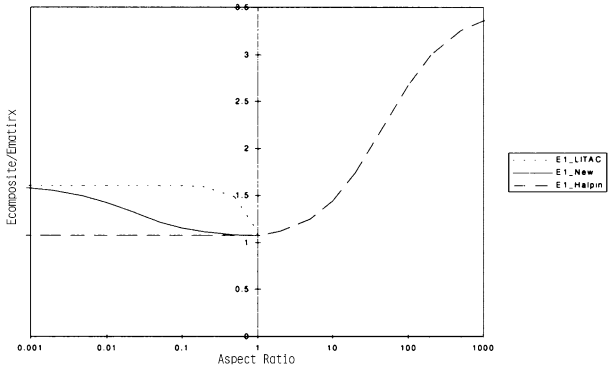

Fig. 11. Refined predictions for E_1 with $E_r = 100$, with a Poisson's ratio of 0.4 for both matrix and filler, and a filler volume fraction of 0.025.

where, as before $E_1(1/\infty)$ is the solution for infinitely thin disks, and $E_1(1)$ is the solution for spheres. Fig. 11 shows the refined predictions for E_1 with $E_r = 100$, a Poisson's ratio of 0.4 for both matrix and filler, and a filler volume fraction of 0.025. This figure clearly demonstrates that revising the method of interpolation removes the irregular behavior of E_1 in the neighborhood of spherical particles.

4.7. Refinements in ν_{12} calculation for disk-shaped particles

Using the LITAC procedure for calculating ν_{12} with the refined procedures described above for calculating E_1 and E_2 yields quite reasonable results, as shown in Fig. 12.

4.8. Examples

We used the equations developed above to predict Young's modulus as a function of the angle between the applied normal stress and the symmetry axis of the platelets. The results of these calculations will now be shown as plots of the ratio of composite Young's modulus to matrix Young's modulus, as a function of orientation angle, for four different aspect ratios. Fig. 13 is for $E_r = 100$, Fig. 14 is for $E_r = 100\,000$. In both figures, $\phi = 0.025$, and Poisson's ratio of both matrix and filler was set to 0.4. Using these new results for elastic constants, we are able to predict the response of Young's modulus of a nanocomposite material to changes in the direction of the applied normal stress. The results show that (a) platelet orientation has a significant effect on Young's modulus, and (b) a minimum value of Young's modulus exists when the particle symmetry axis is about 40° away from the applied normal stress.

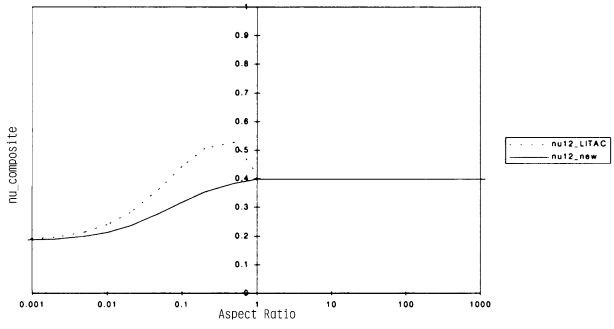

Fig. 12. It is shown that using the LITAC procedure for calculating ν_{12} with the refined procedures for calculating E_1 and E_2 yields quite reasonable results.

5. Discussion

Many books provide detailed and general background information on composite theory. In our opinion, most notable are the books of Nemat-Nasser and Hori [28] for its mathematical thoroughness and of Christensen [29] for its emphasis on the engineering aspects. An article by Tucker et al. [30] with emphasis on the internally consistent combination of a set of judiciously chosen techniques to predict the thermoelastic properties of a wide variety of composites, and the review articles by Ahmed and Jones [31] and Chow [32], provide concise descriptions of models and are recommended to readers interested in relatively brief discussions of several popular models. The thermoelastic properties of platelet-reinforced composites were also addressed in an important manuscript by Christensen [33].

While there is an obvious need for work on the mechanics of nanocomposites, the reader may ask whether continuum mechanics can be applied successfully to materials of such dimensions. Analytical expressions for thermoelastic properties have the advantage of simplicity, but the disadvantage of being generally based on idealized representations of the morphology. It is impossible to use such expressions to predict the full range of variations possible in the thermoelastic properties as a function of the morphology. To be able to use modeling in designing composites with the same confidence as a civil engineer uses calculations to design buildings, the property prediction models must ultimately be able to predict the effects of subtle variations in morphology, such as between models that can be extracted by the automatic meshing of different two-dimensional electron micrographs [34] or predicted by using the recently developed mesoscale simulation methods.

As Vaia and Giannelis [35] emphasized, nanocomposites differ from conventional composites because of their vast interfacial areas per unit volume and the nanoscopic dimensions between the nanoelements. The presence of many chains at interfaces means that much of the polymer is really 'interphase-like' instead of having bulk-like properties. Furthermore, polymer chains are quite often confined between the surfaces of nanoplatelets, which are closer to each other than the radius of gyration of a chain. Both adjacency to a nanoplatelet surface and confinement between such surfaces clearly modify the thermodynamics of polymer chain conformations and the kinetics of chain motions. These two factors may potentially also modify the effective mechanical properties of the polymer. Such modifications could affect the mechanical properties of the nanocomposite

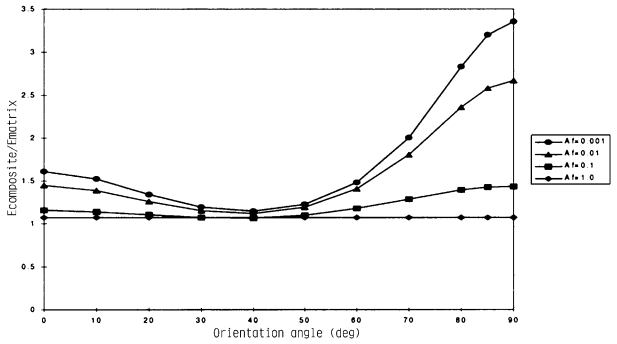

Fig. 13. Young's modulus as a function of the angle between the applied normal stress and the symmetry axis of the platelets, as the ratio of composite Young's modulus to matrix Young's modulus, as a function of orientation angle, for four different aspect ratios, with $\phi = 0.025$, Poisson's ratio of both matrix and filler set to 0.4, and $E_r = 100$.

in ways that are not yet fully understood and perhaps not representable completely adequately by analytical expressions based on continuum mechanics.

Another relevant consideration is that the analytical expressions of micromechanics are generally most accurate at low volume fractions of the 'filler' phase. The details of the morphology become increasingly more important at higher volume fractions. This fact was illustrated by Bush [36] with boundary element simulations of the elastic properties of particulate-reinforced and whisker-reinforced composites. The volume fraction at which such details become more important decreases with increasing filler anisotropy, as was shown by Fredrickson and Bicerano [37] in the context of analytical models for nanocomposite permeability.

Termonia [38] developed a stochastic simulation approach to describe the factors controlling the mechanical properties of short fiber-reinforced composites with variable fiber orientation. His method takes the testing conditions (temperature and deformation rate) into account explicitly within the framework of the kinetic theory of fracture. It thus allows not only the calculation of the elastic properties

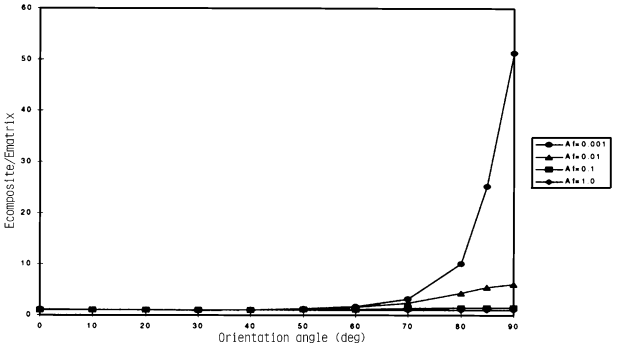

Fig. 14. Young's modulus as a function of the angle between the applied normal stress and the symmetry axis of the platelets, as the ratio of composite Young's modulus to matrix Young's modulus, as a function of orientation angle, for four different aspect ratios, with $\phi = 0.025$, Poisson's ratio of both matrix and filler set to 0.4, and $E_r = 100000$.

of composites but also the calculation of their complete stress–strain curves up to fracture. The main difficulty with its detailed and fully predictive use for designing new materials is in the estimation of the activation energies and activation volumes which are used as input parameters.

Gusev [39,40] developed a generic finite element simulation method for predicting the thermoelastic and transport properties of multiphase materials comprised of anisotropic phases which can be shaped and oriented arbitrarily. Examples of applications of this method have been published for the moduli, coefficients of thermal expansion and dielectric constants of composites with polymeric matrices. Some of the results obtained by using his method (the prediction of much larger potential improvements in the properties of nanocomposites at high nanofiller aspect ratios, and the prediction of three-body effects in the reinforcement in some composites) differ qualitatively from results predicted with analytical expressions. However, these predictions from the numerical simulations will need to be validated with experiments on carefully prepared and well-characterized composite specimens in the future, before the method can be considered to have been fully tested.

The foregoing discussion should make it clear that the analytical expressions of continuum mechanics must be used with caution for nanocomposites. Nonetheless, given the ease and convenience of using such expressions, and the fact that they will continue to be used routinely in practical work whenever quick first estimates of composite behavior are needed, it is important to continue improving such methods. The work reported in this manuscript provides significant improvements compared with existing methods in the ability to predict nanocomposite elastic behavior. It has helped practical experimental work on nanocomposite development by providing semiquantitative estimates of what to expect as well as by elucidating the relative importance of various factors in determining the deviations of the observed reinforcement from its ideal limits. On the other hand, a detailed quantitative comparison with experimental data has been difficult thus far because of the great complexity of nanocomposite morphology and the resulting challenges to its precise characterization in terms of the morphological features sed in the model. Work is in progress in our group to analyze some of the same aspects of nanocomposite elastic behavior with numerical simulations using commercially available software implementing Gusev's method.

6. Summary and conclusions

This paper addressed three important aspects, neglected in all previous literature, of the micromechanics of nanocomposites reinforced by platelet-shaped fillers:

- A model was developed to predict the buckling of platelet-shaped high aspect ratio filler particles in reinforced

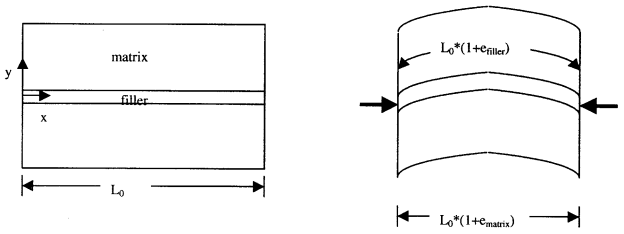

Fig. 15. Schematic representation of undeformed and one possible deformed configuration for a composite under compression.

materials under compressive loading. It predicts a critical strain above which platelet buckling, and hence a reduction in the compressive modulus relative to the tensile modulus, is expected to occur. A simple formula for the critical strain was developed. This formula was used in calculations on a typical polypropylene nanocomposite, for which the critical strain was seen to be sufficiently high for the compressive modulus not to be reduced relative to the tensile modulus.

- A model was developed to account for the reduction of the reinforcement efficiency of clay platelets of high aspect ratio in a polymer matrix as a result of the incomplete exfoliation of platelets into 'pseudoparticle' stacks containing polymer layers sandwiched between successive clay platelet layers rather than into individual perfectly exfoliated and well-dispersed platelets. Such stacks have a lower effective aspect ratio and a lower effective Young's modulus than the completely exfoliated platelets, with these two detrimental effects being only partially contravened by their higher effective volume fractions. It was shown by detailed calculations that incomplete exfoliation has a very significant detrimental effect on the reinforcement efficiency.
- Incomplete exfoliation is just one of the two separate important effects which, in combination, lower the reinforcement efficiency observed in typical nanocomposites significantly relative to the ultimate theoretical limits. A model was also developed for the other important effect, which is the deviation of the platelet orientation from perfect biaxial in-plane. It was shown by detailed calculations that the deviation of the platelet orientation from perfect biaxial in-plane also has a very significant detrimental effect on the reinforcement efficiency.

Acknowledgements

We thank Rich Fibiger, Juan Garcés and Dave Moll for helpful discussions. This work was supported in part by the government of the USA, under Cooperative Agreement No. 70NANB7H3028, awarded by the Department of Commerce, National Institute of Standards and Technology.

Appendix A. Critical strain for onset of buckling during compression

In calculating the critical strain, we assumed that no energy is stored via bending of filler particles. This gives a lower limit for the critical strain (If it becomes important to estimate the critical strain more accurately, it is possible to include the effects of filler stiffness via additional terms in the strain energy function.). With this assumption, the strain energy per unit volume in the filler is simply computed from the filler compressive strain:

$$u_{\text{filler}} = \tfrac{1}{2} E_{\text{filler}} e_{\text{filler}}^2,$$

where u_{filler} is the strain energy per unit volume of filler, E_{filler} the compressive modulus of the filler, and e_{filler} is the compressive strain in the filler.

The strain energy in the matrix is computed from two strain fields; namely, the uniform compressive strain and the shear strain produced by the filler buckling. The strain energy from pure compression of the matrix is:

$$u_{\text{matrix,compression}} = \tfrac{1}{2} E_{\text{matrix}} e_{\text{matrix}}^2$$

where $u_{\text{matrix,compression}}$ is the strain energy per unit volume of matrix, E_{matrix} the compressive modulus of the matrix, and e_{matrix} is the compressive strain in the matrix. The strain energy from the shear strain in the matrix, produced by filler buckling is:

$$u_{\text{matrix,shear}} = \tfrac{1}{2} G_{\text{matrix}} \gamma_{\text{matrix}}^2$$

where $u_{\text{matrix,shear}}$ is the strain energy per unit volume of matrix, G_{matrix} the shear modulus of the matrix, and γ_{matrix} is the shear strain in the matrix due to filler buckling. Buckling is assumed to follow a sinusoidal pattern, with a wavelength parameter λ which takes on whatever value necessary to minimize strain energy.

In order to evaluate the terms of the strain energy function, the compressive strain in the matrix and filler must be related to the amount of buckling in the filler, and the shear strain in the matrix must be computed. In the matrix, deformation normal to the platelets is given by the equation:

$$y = Y + d_y = Y + A \sin\left(\frac{2\pi X}{\lambda}\right),$$

where y is a post-deformation coordinate; X and Y are pre-deformation coordinates; and A and λ are the amplitude and wavelength of the buckling. Fig. 15 shows a schematic of one possible mode of deformation, where the wavelength is twice the length of the filler. The only non-zero shear strain is given by:

$$\gamma_{xy} = \frac{\partial d_x}{\partial Y} + \frac{\partial d_y}{\partial X} = 0 + \left(\frac{2\pi A}{\lambda}\right)\cos\left(\frac{2\pi X}{\lambda}\right),$$

because the X and Z deformations depend only on X and Z, respectively.

To relate the amplitude of the buckling to the compressive

strain in the matrix and filler, let L_0 be the original length of the filler, and L_{def} be the deformed filler length. Then the observation that the difference between the undeformed filler length and the deformed filler length equals the compressive deformation becomes:

$$L_0 - L_{def} = -e_{filler}L_0,$$

or

$$L_0(1 + e_{filler}) = L_{def}$$

$$= \int_0^{L_0 + L_0 e_{matrix}} \sqrt{1 + \left(\frac{2\pi A}{\lambda}\right)^2 \cos^2\left(\frac{2\pi x}{\lambda}\right)}\,dx,$$

where the deformed filler length has been expressed using the standard formula for path length. Changing variables to $\alpha = \frac{2\pi x}{\lambda}$, and using the identity $\lambda n = L_0(1 + e_{matrix})$, the right hand side becomes:

$$\left(\frac{\lambda}{2\pi}\right)\int_0^{2n\pi} \sqrt{1 + \left(\frac{2\pi A}{\lambda}\right)^2 \cos^2\alpha}\,d\alpha$$

$$= \left(\frac{4n\lambda}{2\pi}\right)\int_0^{2\pi} \sqrt{1 + \left(\frac{2\pi A}{\lambda}\right)^2 \cos^2\alpha}\,d\alpha$$

$$= \left(\frac{2n\lambda}{\pi}\right)\sqrt{1 + p^2}E\left(\frac{\pi}{2}, \frac{p}{\sqrt{1 + p^2}}\right)$$

where $p = (2\pi A)/\lambda$ via Eq. 2.614 of Ref. [24] and E is the elliptic integral of the second kind. Putting the right and left sides back together and eliminating n in favor of L_0,

$$L_0(1 + e_{filler}) = \frac{L_0(1 + e_{matrix})}{\pi/2}\sqrt{1 + p^2}E\left(\frac{\pi}{2}, \frac{p}{\sqrt{1 + p^2}}\right).$$

Expressing the terms involving p as a power series yields:

$$1 + e_{filler} = (1 + e_{matrix})\left(1 + \frac{p^2}{2} - \frac{p^4}{4}\cdots\right)$$

$$\times\left(1 - \frac{p^2}{4(1 + p^2)} - \frac{3p^4}{64(1 + p^2)^2}\cdots\right),$$

which gives to leading order,

$$e_{filler} - e_{matrix} = \frac{p^2}{4} = \left(\frac{\pi A}{\lambda}\right)^2.$$

Note that since e_{filler} and e_{matrix} are small, the leading order approximation is justified.

The resulting relationship between buckling and deformation is:

$$A = \frac{\lambda\sqrt{e_{filler} - e_{matrix}}}{\pi},$$

where A is the amplitude of the buckling, and λ is its wavelength. The shear strain in the matrix is:

$$\gamma_{matrix} = \left(\frac{2\pi A}{\lambda}\right)\cos\left(\frac{2\pi x}{\lambda}\right),$$

where x is the coordinate along the direction of the compression. Substituting these results into the expression for $u_{matrix,shear}$ produces:

$$u_{matrix,shear} = 2G_{matrix}(e_{filler} - e_{matrix})\cos^2\left(\frac{2\pi x}{\lambda}\right)$$

To obtain the total strain energy in the composite, the individual portions of the strain energy function are added and integrated over the appropriate regions of the composite:

$$U_{tot} = \int_{V_{matrix}} u_{matrix,compression}\,dV + \int_{V_{matrix}} u_{matrix,shear}\,dV$$

$$+ \int_{V_{filler}} u_{filler,compression}\,dV$$

This produces the following total strain energy per unit volume for the composite:

$$u_{tot} = \tfrac{1}{2}E_{matrix}e_{matrix}^2(1 - \phi)$$

$$+ G_{matrix}(e_{filler} - e_{matrix})(1 - \phi) + \tfrac{1}{2}E_{filler}e_{filler}^2\phi,$$

where ϕ is the volume fraction of filler particles. In the limit of no filler buckling ($e_{matrix} = e_{filler}$), this reduces to the expected result for linear compression of the matrix and filler. It is interesting to note that this expression is independent of λ, the assumed wavelength of the buckling.

To find the minimum energy condition at any given observed strain, e_{matrix}, the derivative of u_{tot} with respect to e_{filler} can be set to zero. This results in:

$$e_{filler,min} = \frac{G_{matrix}(1 - \phi)}{E_{filler}\phi}$$

$$= \left(\frac{E_{matrix}}{E_{filler}}\right)\left(\frac{1}{2(1 + \nu_{matrix})}\right)\left(\frac{1 - \phi}{\phi}\right)$$

When the overall observed strain, e_{matrix}, is greater than the value calculated by using this expression for $e_{filler,min}$, this expression predicts the amount of filler strain, and thus the amount of filler buckling. When the overall observed strain, e_{matrix}, is smaller than the value calculated by using this expression for $e_{filler,min}$, no filler buckling occurs since it would be physically unreasonable for the filler strain to be greater than the overall observed strain. When ($e_{matrix} = e_{filler,min} = e_{crit}$), a critical strain is reached at which filler buckling will start to occur; this is an expression for that critical strain.

Appendix B. Calculation of reinforcement due to stacks of platelets

The aspect ratio of the platelet stack can be evaluated

simply from the geometry: in each platelet stack, there are N platelet layers, and $(N-1)$ inter-platelet layers. If we let L be the long dimension of the platelet, t be the short dimension (thickness) of the platelet, and s be the inter-platelet spacing, then

$$A_f' = \frac{L}{Nt + (N-1)s} = \frac{L}{Nt(1 + (1 - 1/N)\frac{s}{t})}$$

$$= \frac{A_f}{N}\left(\frac{1}{1 + (1 - 1/N)\frac{s}{t}}\right)$$

The volume fraction of the platelet stacks in the matrix can also be simply evaluated from the geometry:

$$\phi' = \frac{V_{\text{platelet-stacks}}}{V_{\text{platelet-stacks}} + V_{\text{outside-platelet-stacks}}}$$

$$= \frac{V_{\text{platelets}} + V_{\text{inter-platelets}}}{(V_{\text{platelets}} + V_{\text{inter-platelets}}) + (V_{\text{matrix}} - V_{\text{inter-platelets}})},$$

$$\phi' = \frac{V_{\text{platelets}}}{V_{\text{platelets}} + V_{\text{matrix}}} + \frac{V_{\text{inter-platelets}}}{V_{\text{platelets}} + V_{\text{matrix}}}$$

$$= \phi + \frac{V_{\text{inter-platelets}}}{V_{\text{platelets}} + V_{\text{matrix}}},$$

and, noting that $V_{\text{matrix}} = V_{\text{platelets}}(1/\phi - 1)$,

$$\phi' = \phi + \frac{V_{\text{inter-platelets}}}{V_{\text{platelets}} + V_{\text{platelets}}(1/\phi - 1)}$$

$$= \phi + \frac{\phi V_{\text{inter-platelets}}}{V_{\text{platelets}}} = \phi\left(1 + \frac{(N-1)sL^2}{NtL^2}\right),$$

$$\phi' = \phi(1 + (1 - 1/N)\frac{s}{t})$$

The ratio of the modulus of the platelet stacks to that of the matrix can be calculated using the geometry of the platelet stacks; and a result from the theory of composites, namely, the effective modulus of a continuously reinforced composite beam:

$$E_{\text{platelet-stacks}} V_{\text{platelet-stacks}}$$

$$= E_{\text{platelets}} V_{\text{platelets}} + E_{\text{matrix}} V_{\text{inter-platelets}},$$

$$E_{\text{platelet-stacks}}(Nt + (N-1)s)$$

$$= E_{\text{platelets}}(Nt) + E_{\text{matrix}}((N-1)s),$$

$$E_r' = \frac{E_{\text{platelet-stacks}}}{E_{\text{matrix}}}$$

$$= \left(\frac{E_{\text{platelets}}}{E_{\text{matrix}}}\right)\left(\frac{Nt}{Nt + (N-1)s}\right) + \frac{(N-1)s}{Nt + (N-1)s},$$

$$E_r' = E_r\left(\frac{1}{1 + (1 - 1/N)\frac{s}{t}}\right) + \frac{(1 - 1/N)\frac{s}{t}}{1 + (1 - 1/N)\frac{s}{t}}.$$

Putting all the above results together results in the following set of equations to predict the composite modulus of an incompletely exfoliated material:

$$\frac{E_{\text{composite}}}{E_{\text{matrix}}} = \frac{1 + 2A_f'\eta'\phi'}{1 - \eta'\phi'}, \qquad \eta' = \frac{E_r' - 1}{E_r' + 2A_f'},$$

$$A_f' = \frac{A_f}{N}\left(\frac{1}{1 + (1 - 1/N)\frac{s}{t}}\right),$$

$$\phi' = \phi(1 + (1 - 1/N)\frac{s}{t}),$$

$$E_r' = E_r\left(\frac{1}{1 + (1 - 1/N)\frac{s}{t}}\right) + \frac{(1 - 1/N)\frac{s}{t}}{1 + (1 - 1/N)\frac{s}{t}}.$$

In addition to the parameters of the 'fully exfoliated' Halpin–Tsai equations, these equations introduce two new parameters: N, the number of platelets in a stack, and s/t, the ratio of the spacing between platelets in a stack to the thickness of a platelet.

We would like these equations to reproduce the results of the familiar 'continuum' version of the Halpin–Tsai equations in a number of limits.

- When $N = 1$, there is only one platelet in a stack. In this case, a simple examination of the equations for A_f', ϕ', and E_r' shows that they become A_f, ϕ, and E_r, respectively, thus recovering the continuum Halpin–Tsai equations.
- When $s/t = 0$, there is no interplatelet layer, so ϕ' and E_r' should be equal to ϕ and E_r (they are); and A_f' and A_f should be related by a factor equal to the number of layers (they are). Again, the continuum equation results are recovered.
- There should be an upper limit for s/t which corresponds to continuum behavior. At this upper limit, the modulus enhancement predicted by the modified equations should equal the modulus enhancement predicted by the continuum equations. From the geometry of the system, s/t in this limit should be $(1 - \phi)/\phi$. The equations above do not demonstrate this limit because the concept of an upper limit to 'stacked' behavior was not built into their derivation (although in practice, the error is not large, e.g. 4% at $N = 5$, $\phi = 0.025$). The following paragraphs detail a modification to the equations to make them self-consistent over the whole range of s/t from 0 to $(1 - \phi)/\phi$.

In comparing the modified Halpin–Tsai equations to the

original continuum version, it is apparent that the modified version approaches the continuum version as N gets close to 1. The simplest way to obtain the correct limiting behavior for s/t, then, is to replace N with a quantity that approaches 1 as s/t approaches $(1-\phi)/\phi$. The quantity must also, of course, approach N at low s/t to maintain the right limiting behavior at low s/t. In addition, to satisfy the first limit in the bullet points above, the quantity must be identically equal to N (for all s/t), when $N = 1$. It is easy to verify that the following replacement for N has all of these properties:

$$\hat{N} = N + (1-N)\left(\frac{s}{t}\right)\left(\frac{\phi}{1-\phi}\right).$$

With this replacement for N, the complete set of equations becomes:

$$\frac{E_{\text{composite}}}{E_{\text{matrix}}} = \frac{1 + 2A'_{\text{f}}\eta'\phi'}{1 - \eta'\phi'}, \qquad \eta' = \frac{E'_{\text{r}} - 1}{E'_{\text{r}} + 2A'_{\text{f}}},$$

$$A'_{\text{f}} = \frac{A_{\text{f}}}{\hat{N}}\left(\frac{1}{1 + (1 - 1/\hat{N})\dfrac{s}{t}}\right),$$

$$\phi' = \phi(1 + (1 - 1/\hat{N})\frac{s}{t}),$$

$$E'_{\text{r}} = E_{\text{r}}\left(\frac{1}{1 + (1 - 1/\hat{N})\dfrac{s}{t}}\right) + \frac{(1 - 1/\hat{N})\dfrac{s}{t}}{1 + (1 - 1/\hat{N})\dfrac{s}{t}},$$

$$\hat{N} = N + (1-N)\left(\frac{s}{t}\right)\left(\frac{\phi}{1-\phi}\right).$$

Appendix C. Aspect ratio dependence of E_1 and E_2 at low volume fraction

The Halpin–Tsai equations are based on *micromechanical solutions* to the elasticity equations, where these equations are solved in three separate regions (one with filler properties, one with matrix properties, and an outer one with the composite properties). Matching boundary conditions between the inner and outer regions provides a built-in way to account for the effects of neighboring filler particles on the local matrix–filler interaction, and thus accounting for concentration effects. By contrast, in the *continuum method*, the elasticity equations are solved in the matrix and filler regions for the given matrix–filler geometry (i.e. there is no 'outer' region, with composite properties) and composite properties are then determined by a suitable volume averaging process. It is easiest to apply the continuum method at very low volume fractions, because one can then use the solution to the elasticity equations for a single filler particle in an infinitely large matrix. When multiple particles are introduced in an effort to account for finite concentrations, the elasticity equations become much more difficult to solve.

We wish to interpolate between the known micromechanics solutions for E_1 for spheres and for infinitely thin disks. Using the continuum approach will show us a way to do this interpolation at low volume fractions, and we will then extend the interpolation method to higher volume fractions. There are two steps to the continuum approach:

1. Find a solution to the elasticity equations. Fortunately, a solution to the elasticity equations exists for a single rigid ellipsoid in an infinite matrix [27]. The result will be reproduced here to correct a number of typographical errors.
2. Volume-average the solution to find the composite properties. The averaging technique is fairly standard, and can be found in many texts on elasticity, fluid mechanics, or electrostatics. As was shown in Ref. [27], the quantity which needs to be volume-averaged to find the compliance tensor components, is the stresslet response to a linear ambient deformation. The stresslet, S_{ij}, which measures the matrix stress response to a strain field, is the coefficient in front of the term

$$\frac{1}{2}\left(\frac{\Im_{ij,k} - \Im_{kj,i}}{16\pi(1-\nu_{\text{m}})G_{\text{m}}}\right),$$

in the solution for the deformation field (Note that in this appendix, S stands for the stresslet, consistent with the notation of Ref. [27]. In the main body of this paper, S stands for the compliance matrix, consistent with the notation in footnote 1). Here, $\Im_{ij,k}$ stands for the derivative in the k direction of the ij component of the fundamental (point force) solution to the elasticity equations,

$$\Im_{ij} = (3 - 4\nu)\frac{\delta_{ij}}{r} + \frac{x_i x_j}{r^3};$$

ν_{m} is the matrix Poisson's ratio; and G_{m} is the matrix shear modulus. To put it another way, if one can find an exact solution for the deformation field in response to a linear ambient deformation, then cast the solution into a form where one of the terms looks like

$$\frac{1}{2}\left(\frac{\Im_{ij,k} - \Im_{kj,i}}{16\pi(1-\nu_{\text{m}})G_{\text{m}}}\right),$$

then the coefficients of that term, when volume averaged, will yield the components of the compliance tensor.

We will first state the solution of the elasticity equations. For an ambient deformation field $u = F^{\infty}\cdot x$, the stresslet for the rigid ellipsoid is in the form $S_{jk} = \bar{S}_{jk} + R\delta_{jk}$, where R represents the isotropic, and $\bar{S}_{jk}$ the deviatoric parts of the

stresslet S_{jk}. R is given by:

$$sR = G_m abc F_{11}^{\infty} \frac{8\pi(1-\nu_m)}{9} \frac{3d_0 + 2s[(2-\alpha_0)\alpha_0'' + 2\beta_0\beta_0'' + 2\gamma_0\gamma_0''] + 4s^2\beta_0\gamma_0}{d_0 + sd_1 + s^2 d_2}$$
$$+ G_m abc F_{22}^{\infty} \frac{8\pi(1-\nu_m)}{9} \frac{3d_0 + 2s[(2-\beta_0)\beta_0'' + 2\gamma_0\gamma_0'' + 2\alpha_0\alpha_0''] + 4s^2\gamma_0\alpha_0}{d_0 + sd_1 + s^2 d_2}$$
$$+ G_m abc F_{33}^{\infty} \frac{8\pi(1-\nu_m)}{9} \frac{3d_0 + 2s[(2-\gamma_0)\gamma_0'' + 2\alpha_0\alpha_0'' + 2\beta_0\beta_0''] + 4s^2\alpha_0\beta_0}{d_0 + sd_1 + s^2 d_2}$$

where $s = 1 - 2\nu$; a, b, and c are the axes of the ellipsoid,

$d_0 = \alpha_0''\beta_0'' + \beta_0''\gamma_0'' + \gamma_0''\alpha_0''$,

$d_1 = \alpha_0\alpha_0''(\beta_0 + \gamma_0) + \beta_0\beta_0''(\alpha_0 + \gamma_0) + \gamma_0\gamma_0''(\alpha_0 + \beta_0)$,

$d_2 = 2\alpha_0\beta_0\gamma_0$

and the α_0, β_0 and γ_0 are elliptic integrals that will be tabulated below.

The deviatoric parts of the stresslet are:

$$\bar{S}_{11} = \frac{32\pi(1-\nu_m)G_m abc}{9} \frac{2\alpha_0''F_{11}^{\infty} - \beta_0''F_{22}^{\infty} - \gamma_0''F_{33}^{\infty}}{d_0 + sd_1 + s^2 d_2} + \frac{32\pi(1-\nu_m)G_m abc}{9} \frac{(1-2\nu)(2\beta_0\gamma_0F_{11}^{\infty} - \gamma_0\alpha_0F_{22}^{\infty} - \alpha_0\beta_0F_{33}^{\infty})}{d_0 + sd_1 + s^2 d_2}$$
$$- \frac{16\pi(1-\nu_m)G_m abc}{9} \frac{(2\alpha_0\alpha_0'' - \beta_0\beta_0'' - \gamma_0\gamma_0'')(F_{11}^{\infty} + F_{22}^{\infty} + F_{33}^{\infty})}{d_0 + sd_1 + s^2 d_2}$$

with the other on-diagonal components obtained by cycling $1 \to 2 \to 3 \to 1$, $\alpha \to \beta \to \gamma \to \alpha$, and $a \to b \to c \to a$. The off-diagonal components are given by:

$$\bar{S}_{12} = \frac{16\pi(1-\nu_m)G_m abc\left[\frac{\alpha_0+\beta_0}{\gamma_0'}\right]\left[\frac{F_{12}^{\infty}+F_{21}^{\infty}}{2}\right]}{3\left[a^2\alpha_0 + b^2\beta_0 + 2(1-2\nu)\frac{\alpha_0\beta_0}{\gamma_0'}\right]},$$

with the other components again obtained by cycling.

In the equations given above, α, β and γ are combinations of elliptic integrals which can be simplified as follows for prolate spheroids ($a > b = c$, $r = a/c$):

$$\alpha_0 = \frac{2r}{(r^2-1)^{3/2}}\log\left(\frac{1}{r-\sqrt{r^2-1}}\right) - \frac{2}{r^2-1},$$

$$\beta_0 = \gamma_0 = \frac{r^2}{r^2-1} - \frac{r}{(r^2-1)^{3/2}}\log\left(\frac{1}{r-\sqrt{r^2-1}}\right),$$

$$a^2\alpha_0' = \frac{2r^6 - 5r^4}{4(r^2-1)^2} + \frac{3r^3}{4(r^2-1)^{5/2}}\log\left(\frac{1}{r-\sqrt{r^2-1}}\right),$$

$$a^2\beta_0' = a^2\gamma_0' = \frac{r^4+2r^2}{(r^2-1)^2} - \frac{3r^3}{(r^2-1)^{5/2}}\log\left(\frac{1}{r-\sqrt{r^2-1}}\right),$$

$$\alpha_0'' = \frac{2r^4+r^2}{4(r^2-1)^2} - \frac{4r^3-r}{4(r^2-1)^{5/2}}\log\left(\frac{1}{r-\sqrt{r^2-1}}\right),$$

$$\beta_0'' = \gamma_0'' = \frac{-3r^2}{(r^2-1)^2} - \frac{2r^3+r}{(r^2-1)^{5/2}}\log\left(\frac{1}{r-\sqrt{r^2-1}}\right)$$

while for oblate spheroids ($a = b > c$, $r = a/c$), the α, β and γ are:

$$\alpha_0 = \beta_0 = \frac{r^2}{(r^2-1)^{3/2}}\arctan(\sqrt{r^2-1}) - \frac{1}{r^2-1},$$

$$\gamma_0 = \frac{2r^2}{r^2-1} - \frac{2r^2}{(r^2-1)^{3/2}}\arctan(\sqrt{r^2-1}),$$

$$a^2\alpha_0' = a^2\beta_0' = \frac{2r^4+r^2}{(r^2-1)^2} - \frac{3r^4}{(r^2-1)^{5/2}}\arctan(\sqrt{r^2-1}),$$

$$a^2\gamma_0' = \frac{5r^2-2}{4(r^2-1)^2} + \frac{3r^4}{4(r^2-1)^{5/3}}\arctan(\sqrt{r^2-1}),$$

$$\alpha_0'' = \beta_0'' = \frac{-3r^2}{(r^2-1)^2} + \frac{r^4+2r^2}{(r^2-1)^{5/2}}\arctan(\sqrt{r^2-1}),$$

$$\gamma_0'' = \frac{r^2+2}{4(r^2-1)^2} + \frac{r^4-4r^2}{(r^2-1)^{5/2}}\arctan(\sqrt{r^2-1})$$

Once the terms of the stresslet have been computed, they can be used to determine the compliance tensor for the composite as follows. In a homogeneous deformation, the effective stress tensor is

$$\langle\sigma_{ij}\rangle = \langle\sigma_{ij}^{\text{matrix}}\rangle + \langle\sigma_{ij}^{\text{particle}}\rangle,$$

where the angle brackets denote a volume average. The stress contributed by the matrix is constant, and is given by

$$\langle\sigma_{ij}^{\text{matrix}}\rangle = \lambda_m\epsilon_{kk}\delta_{ij} + G_m(\epsilon_{ij} + \epsilon_{ji}),$$

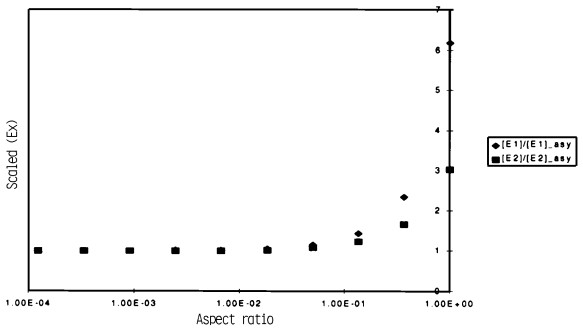

Fig. 16. It is shown that the behaviors of $[E_1]$ and $[E_2]$ as a function of aspect ratio are very similar.

where $\lambda_m = (2\nu_m G_m)/(1 - 2\nu_m)$. The particle-contributed stress is given by

$$\langle \sigma_{ij}^{\text{particle}} \rangle = \frac{1}{V} \sum S_{ij},$$

and since for low volume fraction we can treat each particle in isolation,

$$\langle \sigma_{ij}^{\text{particle}} \rangle = \frac{1}{V} \sum S_{ij} = \frac{N}{V} S_{ij} = \frac{\phi}{V_{\text{particle}}} S_{ij} = \frac{\phi}{(4/3)\pi abc} S_{ij},$$

with the S_{ij} as given above. Putting the particle and matrix contributions together allows us to pick off terms in the fourth order stiffness tensor $\mathbf{C}$ which relates stress to strain ($\sigma = \mathbf{C}\epsilon$), because the strain is easily computed for this particular deformation:

$$\epsilon_{ij} = \frac{1}{2}\left(\frac{\partial u_i}{\partial x_j} + \frac{\partial u_j}{\partial x_i} \right) = \frac{1}{2}\left(\frac{\partial}{\partial x_j}(F_{ik}x_k) + \frac{\partial}{\partial x_i}(F_{jk}x_k) \right)$$

$$= \frac{1}{2}(F_{ij} + F_{ji}) = F_{ij}.$$

Taking as an example the C_{1212} term,

$$C_{1212} = \left. \frac{\langle \sigma_{12} \rangle}{\epsilon_{12}} \right|_{\text{other } \epsilon=0} = \left. \frac{\langle \sigma_{12} \rangle}{F_{12}} \right|_{\text{other } F=0}$$

$$= G_m + \frac{\phi}{(4/3)\pi abc} \left. \frac{S_{12}}{F_{12}} \right|_{\text{other } F=0},$$

$$C_{1212} = G_m + \frac{\phi}{(4/3)\pi abc} \frac{16\pi(1-\nu_m)G_m abc}{3} \times \left[\frac{\frac{\alpha_0 + \beta_0}{\gamma_0'}\left(\frac{1}{2}\right)}{a^2\alpha_0 + b^2\beta_0 + 2(1-2\nu_m)\frac{\alpha_0\beta_0}{\gamma_0'}} \right],$$

$$C_{1212} = G_m + 2\phi(1-\nu_m) \times G_m \left[\frac{\frac{\alpha_0 + \beta_0}{\gamma_0'}}{a^2\alpha_0 + b^2\beta_0 + 2(1-2\nu_m)\frac{\alpha_0\beta_0}{\gamma_0'}} \right]$$

The above equations show how to calculate the 81 terms of the fourth order stiffness tensor. Using formulas[1], these 81 terms can be converted into the 36 stiffness matrix and compliance matrix components used.[1] For example, $C_{66} = 1/S_{66} = C_{1212}$. One minor note in the conversion process is that the notation[1] assumes that the particle symmetry axis is always parallel to the '1' direction, while in Ref. [27] it is parallel to the '1' direction for prolate spheroids, and the '3' direction for oblate spheroids.

Our desire is to determine the behavior of the engineering constant E_1 as a function of aspect ratio, and to find a suitable approximation for it. To help accomplish this, Ref. [25] contains formulas for calculating the 5 independent engineering constants from the 36 stiffness matrix components (reproduced here to correct typographical errors):

$$E_1 = C_{11} - \frac{2C_{12}^2}{C_{22} + C_{23}},$$

$$E_2 = (C_{22} - C_{23})\left(1 + \frac{C_{11}C_{23} - C_{12}^2}{C_{11}C_{22} - C_{12}^2}\right),$$

$$\nu_{12} = \frac{C_{12}}{C_{22} + C_{23}}, \qquad G_{23} = C_{44}, \qquad G_{12} = C_{55} = C_{66}$$

Some caution must, however, be exercised. Our solution for the composite properties assumes dilute behavior. It is very easy to get into the 'non-dilute' regime for high or low aspect ratio particles. To ensure this does not happen, it is more useful to plot so called 'intrinsic' properties, generically defined for the property P as follows:

$$[P] = \lim_{\phi \to 0} \frac{P_{\text{composite}} - P_{\text{matrix}}}{\phi}$$

Using this definition, all of the stiffness matrix results can be written in the form:

$$C_{ij} = C_{ij}^{\text{matrix}} + [C_{ij}]\phi,$$

because all of the C_{ij} are linear in ϕ. Computing the 'intrinsic' engineering constants then requires substituting the C_{ij} into the appropriate formula. $[E_1]$, for example, equals:

$$[E_1] = [C_{11}] - 4\nu_m[C_{12}] + 2\nu_m^2([C_{22}] + [C_{23}])$$

Even plotting these intrinsic properties can be misleading. Since the filler particles are rigid, at high aspect ratios these properties will approach infinity. Since we are interested in the rate of approach to the high aspect ratio asymptote, this asymptote was scaled out. The resulting quantities are

plotted in Fig. 16. From this figure, it is clear that the behaviors of $[E_1]$ and $[E_2]$ as a function of aspect ratio are very similar. Constructing and plotting the interpolating function

$$\left[\frac{E_x(A_f) - E_x(1)}{E_x(1/\infty) - E_x(1)}\right]$$

for both quantities shows that at low volume fraction, the response of the interpolating functions based on $[E_1]$ and $[E_2]$ to changes in aspect ratio is almost identical (this plot is shown as Fig. 7 in the main body of the paper). We make the assumption that this will hold at high volume fractions as well, so that we can use the approximation:

$$INTERP1 = \left[\frac{E_1(A_f) - E_1(1)}{E_1(1/\infty) - E_1(1)}\right] \cong \left[\frac{E_2(A_f) - E_2(1)}{E_2(1/\infty) - E_2(1)}\right] = INTERP2$$

References

[1] Kurauchi T, Okada A, Nomura T, Nishio T, Saegusa S, Deguchi R. SAE Technical Paper Series, No. 910584, from the International Congress and Exposition, held in Detroit (February 25 to March 1, 1991), SAE International, 400 Commonwealth Drive, Warrendale, Pennsylvania 15096-0001, USA.

[2] Kojima Y, Usuki A, Kawasumi M, Okada A, Kurauchi T, Kamigaito O. J Appl Polym Sci 1993;49:1259–64.

[3] Kojima Y, Usuki A, Kawasumi M, Okada A, Kurauchi T, Kamigaito O. J Polym Sci, Polym Chem Ed 1993;31:1755–8.

[4] Yano K, Usuki A, Okada A, Kurauchi T, Kamigaito O. J Polym Sci, Polym Chem Ed 1993;31:2493–8.

[5] Usuki A, Kawasumi M, Kojima Y, Okada A, Kurauchi T, Kamigaito O. J Mater Res 1993;8:1174–8.

[6] Usuki A, Kojima Y, Kawasumi M, Okada A, Fukushima Y, Kurauchi T, Kamigaito O. J Mater Res 1993;8:1179–84.

[7] Kojima Y, Usuki A, Kawasumi M, Okada A, Fukushima Y, Kurauchi T, Kamigaito O. J Mater Res 1993;8:1185–9.

[8] Usuki A, Koiwai A, Kojima Y, Kawasumi M, Okada A, Kurauchi T, Kamigaito O. J Appl Polym Sci 1995;55:119–23.

[9] Kojima Y, Usuki A, Kawasumi M, Okada A, Kurauchi T, Kamigaito O, Kaji K. J Polym Sci, Polym Phys Ed 1995;33:1039–45.

[10] Kawasumi M, Hasegawa N, Kato M, Usuki A, Okada A. Macromolecules 1997;30:6333–8.

[11] Krishnamoorti R, Vaia RA, Giannelis EP. Chem Mater 1996;8:1728–34.

[12] Krishnamoorti R, Giannelis EP. Macromolecules 1997;30:4097–102.

[13] Lan T, Kaviratna PD, Pinnavaia TJ. Proc ACS Div Polym Mater Sci Engng 1994;71:527–8.

[14] Lan T, Pinnavaia TJ. Chem Mater 1994;6:2216–9.

[15] Messersmith PB, Giannelis EP. Chem Mater 1994;6:1719–25.

[16] Laus M, Francescangeli O, Sandrolini F. J Mater Res 1997;12:3134–9.

[17] Vaia RA, Giannelis EP. Macromolecules 1997;30:7990–9.

[18] Vaia RA, Giannelis EP. Macromolecules 1997;30:8000–9.

[19] Balazs AC, Singh C, Zhulina E, Lyatskaya Y. Acc Chem Res 1999;32:651–7.

[20] Ginzburg VV, Singh C, Balazs AC. Macromolecules 2000; 33(1):089–1099.

[21] Bicerano J, Douglas JF, Brune DA. J Macromol Sci, Rev Macromol Chem Phys, C 1999;39:561–642.

[22] Hoff NJ, Mautner SE. J Aero-Sci 1945;12:285–97.

[23] Hollaway L. Polymer composites for civil and structural engineering. London: Blackie Academic and Professional, 1993.

[24] Gradshteyn IS, Ryzhik IM. Table of integrals, series, and products. Orlando: Academic Press, 1980.

[25] Halpin JC, Kardos JL. Polym Engng Sci 1976;16:344–52.

[26] Halpin JC. Primer on composite materials analysis. 2nd ed. Lancaster, PA: Technomic Publishing, 1992.

[27] Phan-Thien N, Kim S. Microstructures in elastic media, preprint obtained via personal communication.

[28] Nemat-Nasser S, Hori M. Micromechanics: Overall properties of heterogeneous materials. New York: North-Holland, 1993.

[29] Christensen RM. Mechanics of composite materials. New York: Wiley, 1979.

[30] Camacho CW, Tucker III CL, Yalvac S, McGee RL. Polym Compos 1990;11:229–39.

[31] Ahmed S, Jones FR. J Mater Sci 1990;25:4933–42.

[32] Chow TS. J Mater Sci 1980;15:1873–88.

[33] Christensen RM. J Engng Mater Technol 1979;101:299–303.

[34] Langer SA, Fuller Jr. ER, Carter WC. Comp Sci Engng 2001;3(3):15–23.

[35] Vaia RA, Giannelis EP. MRS Bulletin 2001:394–401.

[36] Bush MB. Mater Sci Engng, A 1992;154:139–48.

[37] Fredrickson GH, Bicerano J. J Chem Phys 1999;110:2181–8.

[38] Termonia Y. J Polym Sci, Polym Phys Ed 1994;32:969–79.

[39] Gusev AA. Macromolecules 2001;34:3081–93.

[40] Gusev AA, Slot JJM. Adv Engng Mater 2001;3:427–9.